JGR Earth Surface

RESEARCH ARTICLE
10.1029/2020JF005558

Sediment Delivery to a Tidal Marsh Platform Is Minimized by Source Decoupling and Flux Convergence

Daniel J. Coleman[1], **Neil K. Ganju**[2], **and Matthew L. Kirwan**[1]

[1]William & Mary, Virginia Institute of Marine Science, Gloucester Point, VA, USA, [2]Woods Hole Coastal and Marine Research Center, U.S. Geologic Survey, Woods Hole, MA, USA

Key Points:
- A detailed record of suspended sediment concentration illustrates a time scale-dependent relationship between marsh and channel
- Flux convergence suggests sediment trapping near the marsh edge results in minimal sediment delivery to the marsh interior
- Decoupling of marsh and channel sediment supplies makes predicting marsh vulnerability from channel sediment concentration difficult

Supporting Information:
- Supporting Information S1

Correspondence to:
D. J. Coleman,
djcoleman@vims.edu

Citation:
Coleman, D. J., Ganju, N. K., & Kirwan, M. L. (2020). Sediment delivery to a tidal marsh platform is minimized by source decoupling and flux convergence. *Journal of Geophysical Research: Earth Surface*, *125*, e2020JF005558. https://doi.org/10.1029/2020JF005558

Received 3 FEB 2020
Accepted 23 JUL 2020
Accepted article online 27 JUL 2020

©2020. American Geophysical Union. All Rights Reserved.

Abstract Sediment supply is a primary factor in determining marsh response to sea level rise and is typically approximated through high-resolution measurements of suspended sediment concentrations (SSCs) from adjacent tidal channels. However, understanding sediment transport across the marsh itself remains limited by discontinuous measurements of SSC over individual tidal cycles. Here, we use an array of optical turbidity sensors to build a long-term, continuous record of SSC across a marsh platform and adjacent tidal channel. We find that channel and marsh concentrations are correlated (i.e., coupled) within tidal cycles but are largely decoupled over longer time scales. We also find that net sediment fluxes decline to near zero within 10 m of the marsh edge. Together, these results suggest that large sections of the marsh platform receive minimal sediment independent of flooding frequency or channel sediment supply. Marsh-centric, as opposed to channel-centric, measures of sediment supply may better characterize marsh platform vulnerability.

Plain Language Summary Coastal marshes are important for storm surge protection, water filtration, and habitat for wildlife. These environments are at risk of drowning by sea level rise and therefore must build elevation to survive. The material for building elevation can come as sediment suspended in the water, which then settles on the surface of the marsh. We often predict how much elevation a marsh can build by the amount of sediment in the associated tidal channel. However, we found sediment concentration in the channel to be a poor indicator of the amount of sediment reaching the marsh, especially farther from the marsh edge. This is partly because the channel and marsh are decoupled, meaning as the amount of sediment in the channel increases, the amount reaching the marsh does not necessarily increase. We suggest that sediment concentration should be measured directly in the water atop the flooded marsh to best predict how a marsh will survive into the future.

1. Introduction

Accelerating sea level rise (SLR) and decreased sediment supply threaten coastal ecosystems throughout the world, as many deltas, marshes, mangroves, and barrier islands rely on sediment to survive rising sea level (Blum & Roberts, 2009; Ellison & Stoddart, 1991; Fitzgerald et al., 2006; Syvitski et al., 2009; Weston, 2014). Marsh formation and collapse have both been linked to changes in sediment supply (Day et al., 2007; Gunnell et al., 2013; Kirwan et al., 2011; Tommasini et al., 2019; Tweel & Turner, 2012), making coastal marshes a striking example of a system dependent on mineral sediment availability. Sediment supply is a primary factor in vertical accretion rates (Jankowski et al., 2017) and lateral changes in marsh size (Ganju et al., 2017), thereby affecting marsh vulnerability to SLR (Kirwan et al., 2010). Organic accretion is unlikely to allow marshes to survive rapid SLR (Morris et al., 2016), which is consistent with extensive interior marsh loss far from sediment sources (D'Alpaos & Marani, 2016; Schepers et al., 2016; Zhang et al., 2019). Quantifying sediment supply to the marsh platform is therefore crucial in determining salt marsh response to SLR.

How best to characterize sediment supply remains unclear. Numerical models often parameterize sediment supply with an average suspended sediment concentration (SSC) measured in the adjacent tidal channel (Fagherazzi et al., 2012; Kirwan et al., 2010; Ratliff et al., 2015). However, conditions for sediment entrainment often differ from those necessary for overmarsh transport (Duvall et al., 2019). The sediment reaching the marsh may also differ in magnitude and grain characteristics from what is found in the channel (Poirier

et al., 2017). For example, sediment concentration can vary by several orders of magnitude over a single tidal cycle (Christiansen et al., 2000). The pattern of flocculation and grain size varies with tidal stage and on longer time scales both in the channel and across the marsh platform (Chen et al., 2005; Murphy & Voulgaris, 2006; Poirier et al., 2017; Voulgaris & Meyers, 2004). Furthermore, a marsh can succumb to SLR and wave erosion even if the SSC in the channel is high (Ganju et al., 2015). Although tidal channels are the ultimate source of sediment to most tidal marshes (Friedrichs & Perry, 2001; Reed et al., 1999) and are often measured continuously, measurements on the marsh itself are almost entirely collected through bottle sampling (e.g., Christiansen et al., 2000; Leonard & Reed, 2002; Moskalski & Sommerfield, 2012; Poirier et al., 2017; Wang et al., 1993). In this method, a water sample is collected either by hand or an automated sampler at some depth in the water column and taken to the lab for analysis of total suspended sediments, often through vacuum filtration. In part because bottle sampling is labor intensive, samples are typically collected over only a small number of individual tidal cycles. Therefore, it remains uncertain how well marsh sediment availability can be predicted from measurements of SSC in channels alone.

Here, we continuously measure SSC over two growing seasons (8 months total) across a marsh platform and adjacent tidal channel in the Plum Island Estuary. We find that channel and marsh SSC are largely decoupled through time and that sediment fluxes decline with distance from the marsh edge. Ultimately, our findings suggest that measurements of SSC directly on the marsh platform may be required to characterize sediment supply.

2. Methods

2.1. Study Area and Approach

This study was conducted at a mixed *Spartina patens-S. alterniflora* salt marsh in the Plum Island Estuary, a Long Term Ecological Research site in Massachusetts, USA (Figure 1). Marshes in the Plum Island Estuary are vulnerable to SLR as they are bounded by steep uplands that prevent migration and receive limited sediment inputs for vertical soil accretion (Farron et al., 2020; Langston et al., 2020). The system is dammed along the major tributaries and therefore typically has low SSC (median = 15.6 mg/L), which increase to 30–40 mg/L at the estuarine turbidity maximum (Cavatorta et al., 2003; Hopkinson et al., 2018). Sediment budgets for marsh accretion indicate that oceanic input and tidal flat erosion are the largest sources of sediment, followed by marsh edge erosion and then river inputs (Hopkinson et al., 2018). Mean sea level (MSL) and mean higher high water (MHHW) are located at −0.09 and 1.25 mNAVD88, respectively (Millette et al., 2010). The average tidal range is 2.9 m, and approximately 75% of marshes are considered high marsh (Milette et al., 2010). Real-time kinematic global position satellite (RTK GPS) surveys indicate our site was located between 1.19 and 1.70m NAVD88, which corresponds with the transition from low to high marsh in this system (Figure 2; Millette et al., 2010). In many locations, including our site, there is a large marsh escarpment which regularly exceeds 2 m in height (Figure 2). The study site floods from the marsh channel (West Creek) edge to the marsh interior (Law's Point; Figure 1).

We quantified spatial and temporal patterns of suspended sediment transport over two growing seasons (May–November 2016 and June–September 2017) using an array of optical-backscatter turbidity sensors equipped with automatic antifouling wipers. We were not able to collect measurements or draw conclusions during the winter months when sediment transport is influenced by ice rafting, rather than simple advection of SSC (Argow et al., 2011). We deployed the sensors across the marsh platform and adjacent tidal channel in a shore-normal transect. Based on direct observations of flooding, we concluded the sensor transect was parallel to the direction of initial marsh flooding. The sensor in the channel (RBR Duo equipped with Seapoint turbidity probe) was located 35 cm above the bed and 3 m from the edge of the marsh. Sensors on the marsh were fastened to rigid grates installed flush with the marsh soil surface. The actual sensor window was located 7 cm above the surface, and the sampling point is 5 cm in front of the sensor window. To minimize interference with plants, we removed vegetation from within this distance and placed a ceramic tile on the ground to prevent regrowth directly in front of the sensor window. In 2016, sensors were placed at 2.7 and 17 m from the marsh edge (RBR Solo and RBR Duo, respectively). In 2017, five sensors were installed on the marsh surface at 1.25 m (RBR Solo), 2.7 m (RBR Duo), 9.3 m (RBR Duo), 17 m (YSI 6600), and 24 m (YSI Exo) from the marsh edge (Figure 1). The sensor located 17 m into the marsh in 2017 malfunctioned and did not record data. All other sensors measured turbidity every 15 min for the entire deployment,

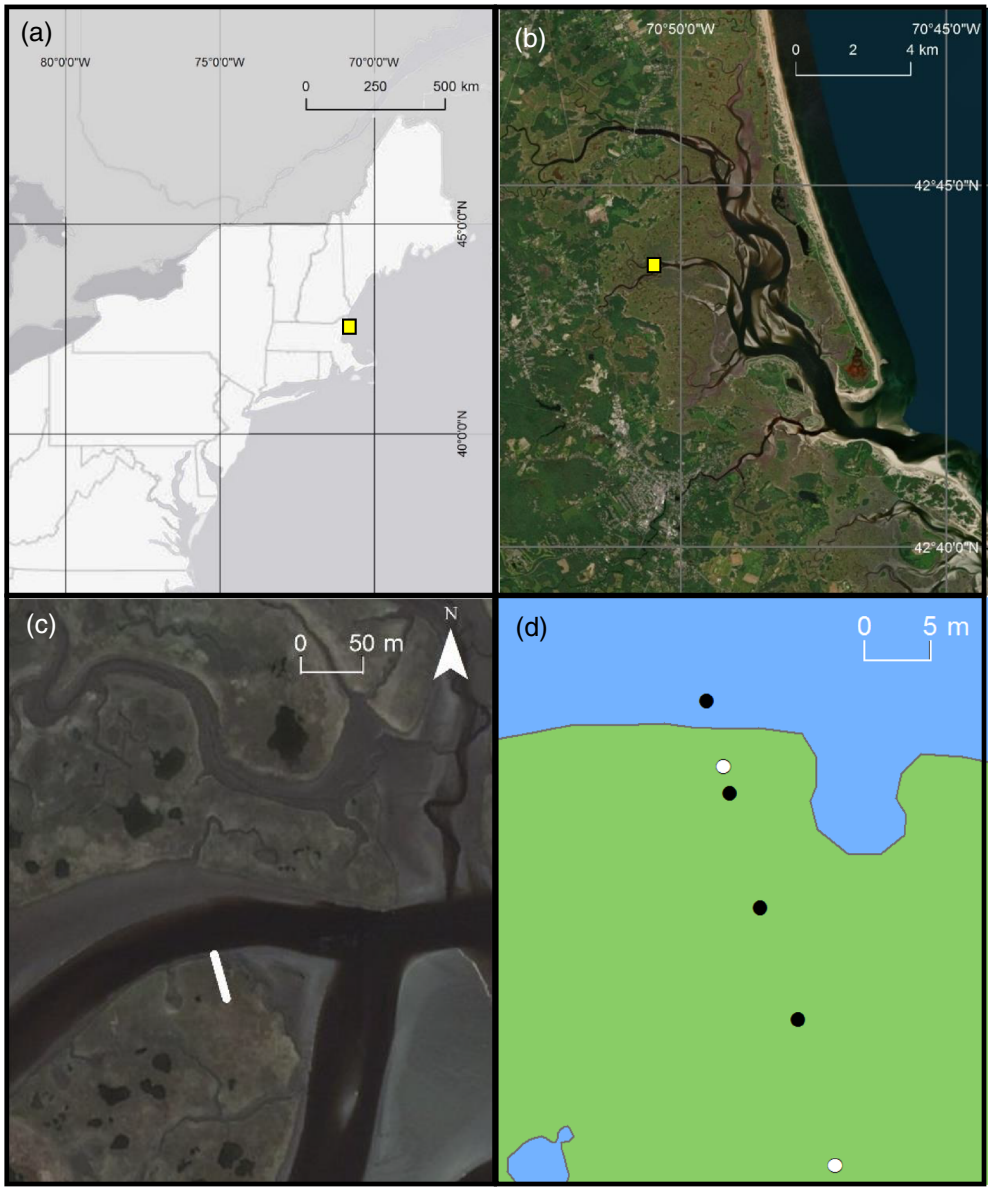

Figure 1. (a) Map of the northeast of the United States, showing location of Plum Island Estuary in the yellow square. (b) Map of the Plum Island Estuary showing the study site in the yellow square. Extensive sand flats downstream of the study site are visible. (c) Regional scale map of the Laws Point study site with sensor transect (white line). (d) Detailed site map showing transect from West Creek into the marsh interior, where black circles represent turbidity sensors with pressure transducers and white circles represent turbidity sensors without pressure transducers. The turbidity sensor located at 17 m inland malfunctioned in 2017 and did not record data. All turbidity sensors on the marsh platform were positioned 7 cm above the bed.

totaling nearly 100,000 measurements, with select sensors also measuring pressure (see Figure 1). The sensor error in turbidity measurements is <2% and significant sensor drift is uncommon (http://seapoint.com/pdf/stm_ds.pdf).

Suspect data points were removed from the time series record following Ganju et al., 2005. We used a recursive filter to remove points which were greater than 10 nephelometric turbidity units (NTU) higher than adjacent time steps. The record was visually analyzed to ensure points being removed represented values anomalously higher than surrounding values. These removed data points represent times when a sensor was obstructed, fouled, or not submerged. Tidal stage and flooding durations were determined

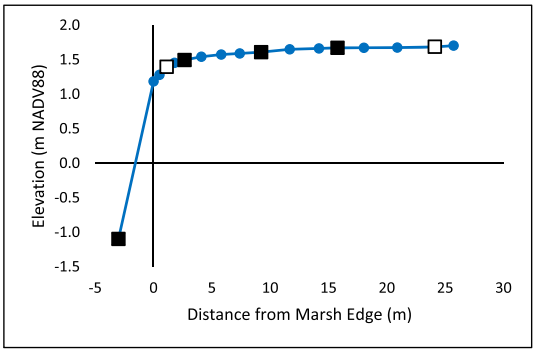

Figure 2. The elevation of the marsh platform via RTK GPS measurements. The squares indicate the location of sensors, with black filled squares indicating sensors also equipped with a pressure sensor. The blue points are additional RTK survey points that did not correspond to a sensor location. The steep slope between the channel sensor and the marsh edge is indicative of the large marsh escarpment common in the system.

by measurements of water level by the sensors themselves (see Figure 2). Specifically, sensors measure pressure which is then corrected for atmospheric pressure obtained from the PIE LTER (Giblin, 2017, 2018). These measurements of water level include astronomical tides and any other environmental drivers affecting water level, for example, wind. Data points were removed when the water level as measured in the channel (in NADV88) was below the sensor elevation (in NADV88). Additionally, we divided the record into flooding tides (increasing water level) and ebbing tides (decreasing water level). We calculated the flood-ebb differential for each sensor by taking the average of all points that occurred during the flooding tide and subtracting the average of all points that occurred during the ebbing tide. There was a slight tidal asymmetry at the site with flood tides comprising 54% of the monitoring duration and ebb tides comprising 46%. Flood-ebb differentials were time weighted to account for this asymmetry following Nowacki and Ganju (2019).

Turbidity data were converted to SSC via laboratory calibrations using sediment collected from the site and in situ field sampling. In the lab, we created sediment-water slurries with a range of SSC and measured them with an additional turbidity sensor. In the field, we measured turbidity with an additional sensor at various locations around the site and at different tidal stages. We collected a water sample in conjunction with each turbidity measurement. This ensures that the calibration is accurate to the average sediment characteristics from across the site. We compared sensor turbidity measurements to total suspended solid measurements obtained via vacuum filtration of water samples and sediment-water slurries. The y intercept value was set to 0, resulting in the equation SSC (mg/L) = 2.26*Sensor Turbidity (NTU) (R^2 = 0.98, n = 32, $p \ll 0.001$; supporting information Figure S2). The average error is 19% over the entire data range and 21% for SSC less than 100 mg/L (supporting information Figure S2). There were no outliers that suggest that the sediment across the site had similar optic properties. All field sensors were in turn individually calibrated to the sensor used in the lab via turbidity standards. In other words, all turbidity sensors were calibrated to one sensor which was then used to calibrate to SSC. Full SSC time series can be found in Figure 3 and online (at doi:10.6073/pasta/d3a96e0db54f4c66899e82e6641ab42b).

2.2. Analytical Methods

We quantified the dispersion of the distribution of SSC of the entire available record for each sensor to quantify how temporal variability in SSC changes with distance into the marsh. We calculated the quartile coefficient of dispersion, which is a nondimensional measure of how spread out a distribution is. Values closer to 0 indicate a tighter or more uniform distribution and values closer to one indicate a more dispersed distribution. Additionally for each sensor, we calculated the difference between the mean concentration and the median concentration normalized by dividing by the mean. Relative mean-median difference values that are closer to 0 would indicate a more uniform or linear normal distribution, whereas values approaching positive one would indicate more points exist in the right tail of the distribution. We determined how both nondimensional measures of dispersion changed with distance via a linear regression.

To identify how coupling between channel and marsh sediment supply varies with time, we compared SSC under various temporal averaging windows from three geomorphic locations: channel, marsh edge, and marsh interior. We defined the marsh edge in 2017 as the average of the sensors located at 1.25 and 2.7 m and the marsh interior as the average of the sensors located at 9.3 and 24 m. For each 15-min increment within a tidal cycle, we averaged data from both years by location. From this, we also created heat density maps to visualize concentration within a tidal cycle by determining the number of data points that were within bins defined by 0.5 mg/L × 15 min. We compared the average concentration per stage in the tidal cycle for the three different geomorphic zones via linear regressions between simultaneous SSC series. For larger temporal windows (i.e., each tidal cycle, day, week, spring-neap cycle, and month) we used all data from both years when all sensors were flooded. For example, to calculate daily average SSC for the channel to compare to daily average SSC for the marsh edge, we remove all points from the channel SSC record when

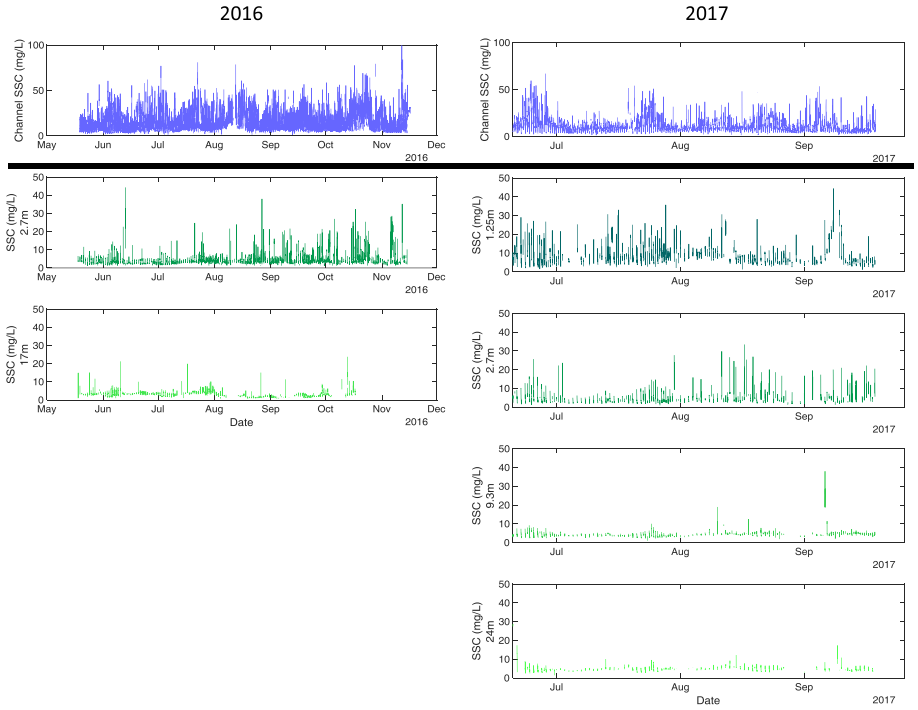

Figure 3. SSC through time for all channel and marsh sensor locations in 2016 (left) and 2017 (right). Records from the channel are shown above the thick, black line in blue, and records from the marsh platform are shown below the thick, black line in progressively lighter green, representing progressively more inland marsh. Note that vertical scale is different between the channel and marsh locations due to larger magnitude of SSC in the channel. Labels on the *y* axis describe distance from the marsh channel edge.

the marsh edge is not flooded. We conducted a linear regression for the time-series of SSC in the three geomorphic zones for all time averaging windows. This was repeated including only flooding tides and only ebbing tides.

In 2016, we harvested plant biomass in replicate plots ($n = 3$) of 0.0625 m^2 within 1 m of each marsh sensor location at equipment deployment, retrieval, and two additional times in between. There was no significant difference in biomass between sampling locations on the marsh platform (analysis of variance, ANOVA, $p = 0.58$), so we compared marsh average biomass to the percent decrease in SSC from the channel to the marsh edge, the marsh edge to the marsh interior, and the channel to the marsh interior. We targeted sampling windows for SSC that were centered on the biomass sampling dates. The analysis consisted of three linear regressions between (1) biomass and average percent decrease in SSC from the channel to the marsh edge, (2) biomass and percent decrease in SSC from the channel to the marsh interior, and (3) biomass and percent decrease in SSC from the marsh edge to the marsh interior. We also conducted a two-dimensional correlation test between the biomass versus time curve and each percent decrease in SSC versus time curves. To account for biomass sampling at the beginning and end of the monitoring, we performed our analysis for numerous different sampling schemes, given in supporting information Table S1. All the sampling schemes produced similar results, suggesting that the results are not an artifact of a particular sampling window.

3. Results

3.1. Broad-Scale Patterns

SSCs decreased from the channel toward the marsh interior (Figure 4). Channel average SSC was 13.6 mg/L ± 9.19 (mean ±σ) compared to an average marsh concentration of 5.24 mg/L ± 4.12. The spatial pattern of SSC appeared to be an exponential decay to a nonzero background concentration in both 2016 and 2017 (Figure 4a). We utilize a natural logarithmic transformation of the data so that we can statistically test the fit of an exponential function with a nonzero background value. The log transformation of the average

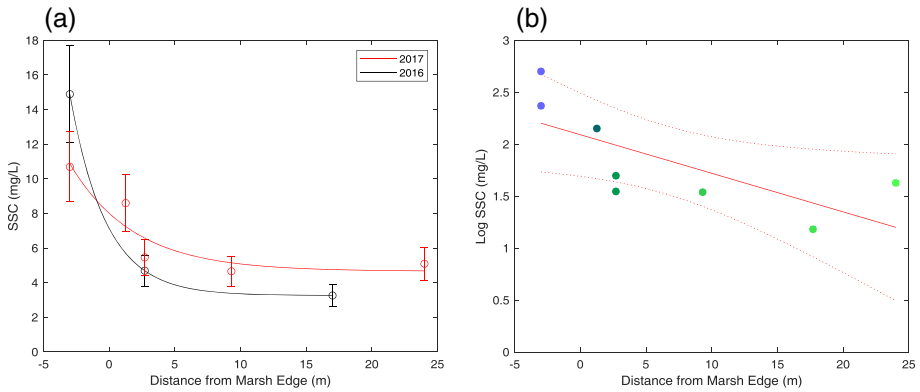

Figure 4. (a) Mean suspended sediment concentration at each sensor location for the entire record of a given year. Error bars represent 95% confidence interval of SSC calibration and the lines indicate best fit exponential decay curves. (b) Log of the average SSC decreases significantly with distance into the marsh edge, with dashed lines representing 95% confidence interval ($R^2 = 0.52$, $p < 0.05$).

concentration for all sensors was significantly correlated with distance from the channel ($R^2 = 0.52$, $p < 0.05$; Figure 4b).

The nondimensional measures of dispersion were largest in the channel and decreased with distance into the marsh. (Figure 5). This means a greater number of measurements are closer in value to the mean (in a nondimensionalized sense) with distance inland. Both the quartile coefficient of dispersion and the relative mean-median difference had a significant linear relationship with distance ($R^2 = 0.54$, $p < 0.05$; $R^2 = 0.61$, $p < 0.05$, respectively).

The difference between average concentrations on flood tides versus that on ebb tides is a predictor of net sediment supply to the marsh complex (French et al., 2008; Ganju et al., 2017). We therefore divided the SSC records into flooding and ebbing tidal components using measured water level to determine the average flood-ebb differential. Overall, the flood-ebb differential is positive and relatively small for each sensor (Figure 6). The differential in the channel is 1.8 mg/L and decreases exponentially with distance into the marsh to approximately 0.15 mg/L (log-transformed, $R^2 = 0.61$, $p < 0.05$; Figure 6).

3.2. Correlations Between Channel and Marsh

The average of all tidal cycles indicates that the channel and the marsh SSC are generally coupled within the tidal cycle time scale, for example, sediment concentrations on the marsh reflect concentrations in the channel (Figure 7). Values at all three locations decrease on the rising tide, reaching a minimum at slack high tide

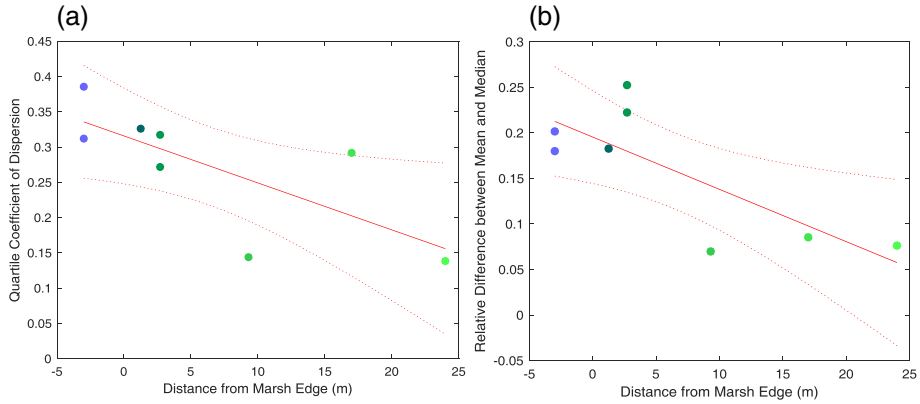

Figure 5. (a) Quartile coefficient of dispersion decreases significantly with distance ($R^2 = 0.54$, $p < 0.05$). (b) The relative mean-median difference for each sensor decreases significantly with distance into the marsh ($R^2 = 0.61$, $p < 0.05$). Dashed lines represented the 95% confidence intervals.

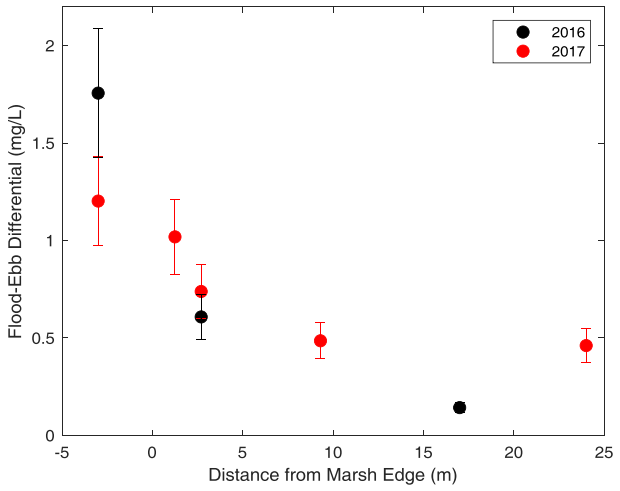

Figure 6. The difference between flood and ebb SSC decreases with distance into the marsh for both 2016 (black) and 2017 (red). Concentrations represent averages of the entire record available for each sensor, ranging from 350 tides at the 2016 channel sensor to 104 tides at the farthest interior sensor in 2017. Error bars represent the 95% confidence interval of SSC calibration. The sediment flux converges (indicating deposition) when the flood-ebb differential at one sensor location is larger than that of the next, more interior, sensor location.

for the channel and marsh edge (Figure 7). The concentrations increase on the falling tide except for in the marsh interior. SSC concentrations are significantly correlated between the channel and marsh edge ($R^2 = 0.58$, $p < 0.05$) and between the marsh edge and marsh interior ($R^2 = 0.52$, $p < 0.05$), but not between the channel and marsh interior ($p = 0.9$). This indicates general coupling of SSC between channel and marsh over individual tidal cycles.

At larger temporal scales (full tidal cycle to monthly), the channel and the marsh demonstrate decoupling, where marsh sediment concentrations do not reflect concentrations in the channel (Figure 8). Linear regressions between channel SSC and marsh edge or marsh interior SSC are either insignificant or significantly negatively correlated for all time averaging windows of interest (Figure 8 and supporting information Figure S5). Decoupling is illustrated in both cases: Negative significant correlations mean that as channel SSC increases, marsh SSC decreases, and insignificant correlations mean that marsh SSC does not increase as channel SSC increases. In contrast, average SSC at the marsh edge is positively correlated to the marsh interior over tidal cycles ($p < 0.05$), daily ($p < 0.05$), weekly ($p < 0.1$), spring-neap cycles ($p < 0.05$), and monthly time scales ($p < 0.1$, supporting information Figure S5). This pattern is also consistent for either only rising tides or only falling tides (supporting information Table S2).

Biomass varied seasonally and was strongly correlated with the proportional decrease in SSC from the channel to the marsh interior (all sampling schemes: $p < 0.05$) and marsh edge to marsh interior (three sampling schemes: $p < 0.05$, one sampling scheme: $p < 0.1$; Figure 9a). Biomass did not significantly correlate with the

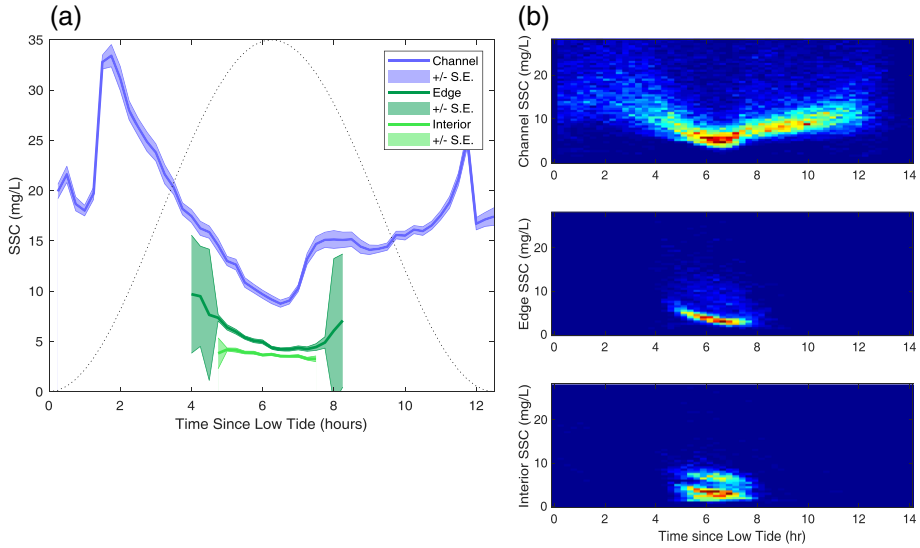

Figure 7. Relationship between SSC and tidal stage for different portions of the marsh channel system. Data represents the average of all measurements over two growing seasons for a given tidal stage. (a) Average SSC for each 15-min increment in the tidal cycle for the channel (blue), marsh edge (dark green), and marsh interior (light green) with envelopes representing one standard error. Superimposed is a hypothetical water level curve (dotted line). Only tidal stages with available data from at least 50 tidal cycles are included. The SSC is statistically significantly related via linear regressions between the channel to the marsh edge ($R^2 = 0.58$), and the marsh edge to the marsh interior ($R^2 = 0.52$), but not the channel to the marsh interior. (b) Heat density map of concentrations over a tidal cycle, where warmer colors represent a higher number of data points that fall within a given 0.5 mg/L by 15-min bin.

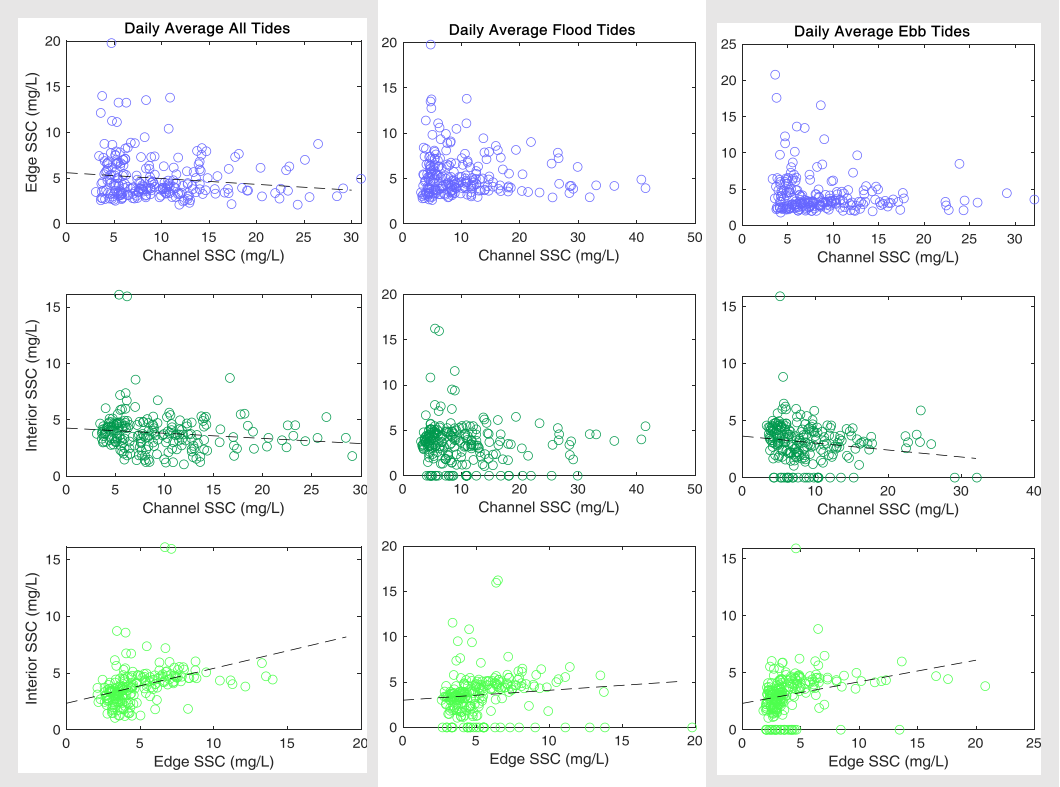

Figure 8. Each point represents a daily averaged concentration only including time points when both sensors being compared were inundated. For example, to calculate the daily average SSC for the channel to compare to the daily average SSC of the marsh edge, we first remove all points when the channel is flooded but the marsh edge is not. Dashed lines represent the best fit linear regression when significant. The first column of graphs includes data for both flooding and ebbing tides, while the second and third columns only include data collected during flooding tides and ebbing tides, respectively. The daily average SSC in the channel does not have a significant positive correlation with the daily average SSC in the marsh regardless of which tides are analyzed. In contrast, daily average marsh edge SSC is significantly positively related to the daily average marsh interior SSC for all tides.

percent decrease of SSC from the channel to the marsh edge in three of the four sampling schemes ($p > 0.1$) and was marginally correlated in one sampling scheme ($p < 0.1$).

4. Discussion

4.1. Spatial Patterns of Suspended Sediment Transport

Our general findings are consistent with previous work in the system suggesting Plum Island Estuary marshes have a limited sediment supply. The average SSC in the tidal channel at our site (13.6 ± 0.07 mg L^{-1}, mean ± SE) is similar to previous measurements in the system, especially those from similar distances upstream (~15 mg/L, Cavatorta et al., 2003; 15.6 mg/L ± 3.6, median ± SE, Hopkinson et al., 2018). Sediment budgets indicate that seaward sediment sources, that is, the ocean and eroding tidal flats in Plum Island Sound, are a more important source of sediment than rivers (Hopkinson et al., 2018). This seaward sediment source is consistent with our observations of a positive flood-ebb differential in the tidal channel, where flood tides would bring the oceanic and tidal flat sediment into the marsh and therefore have higher SSC than river-influenced ebb tides (Figure 6).

Our high-resolution measurements support previous studies but also lead to new insight that cannot be captured with more conventional sampling methods. For example, our study is consistent with the paradigm that SSC is higher in tidal channels and decreases with distance into the marsh (Christiansen et al., 2000; Leonard & Reed, 2002; Poirier et al., 2017). However, continuous sampling allows us to identify that concentrations in the channel have a more disperse distribution than concentrations on the marsh platform

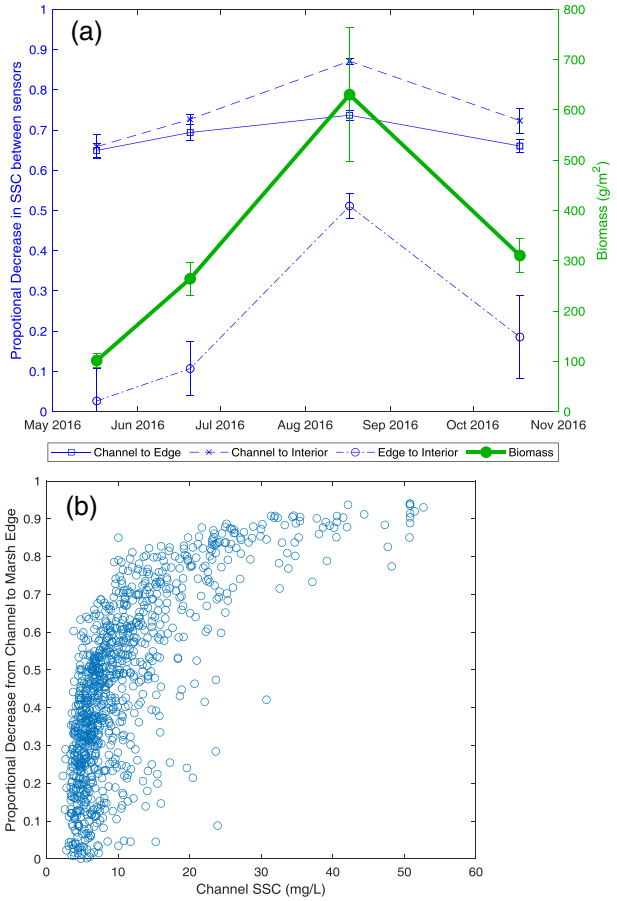

Figure 9. Potential mechanisms for observed spatial patterns in sediment transport. (a) Proportional decrease in SSC was calculated over 2-week periods before and after biomass sampling dates (where possible). Platform-average biomass (green line, right axis) is significantly related to the proportional decrease in SSC from the channel to the marsh interior ($R^2 = 0.99$, x dashed line, left axis) and from the marsh edge to the marsh interior ($R^2 = 0.98$, circle dash-dotted line, left axis). The change in SSC from the channel to the edge ($R^2 = 0.90$, square solid blue line, left axis) is at most marginally correlated with biomass. Error bars represent standard error. (b) Each point represents the channel concentration and proportional decrease from the channel to the marsh edge at a single measurement point during a flooding tide. At higher channel concentrations, there is a larger decrease in SSC between the channel and marsh, indicating that a smaller proportion of channel sediment is transported to the marsh.

(Figure 5). Like many other studies, we find vegetation has an important control on SSC (Coleman & Kirwan, 2019; Leonard & Reed, 2002; Li & Yang, 2009; Temmerman et al., 2005), particularly in controlling the decrease in SSC into the marsh interior (Figure 9a). However, we find that changes in SSC from the channel to the marsh edge do not vary as strongly with plant biomass, suggesting that vegetation is less important near channel edges (Figure 9a). This is perhaps because the hydrodynamic effect of the vegetation is overwhelmed by the effect of channelized flow overtopping the high escarpment.

Our measurements also suggest flux convergence across the marsh platform (Figure 6). Previous work has shown that sediment flux is proportional to the flood-ebb SSC differential, even in the absence of flow velocity measurements (French et al., 2008; Ganju et al., 2017; Nowacki & Ganju, 2019). Sediment flux is said to converge when there is a greater flux into a region than out of the region (Dickhudt et al., 2009; Harris et al., 2008). For example, the point at 2.7 m has a flood-ebb SSC differential of +0.7 mg/L, while the point at 9.3 m has a differential of +0.5 mg/L in 2017 (Figure 6). This indicates that the site has a greater influx of sediment at 2.7 m than at 9.3 m, thus suggesting convergence and net sediment deposition in that region. Overall, the observed sediment flux is small and rapidly declines with distance inland (flood-ebb differential <0.5 mg/L after the first 10 m, Figure 2). The gradient is much greater along the marsh edge than in the interior, suggesting that more sediment is being trapped close to the channel and the marsh interior is largely—but not completely—deprived of mineral sediment.

Strong sediment flux convergence near tidal channel edges would be expected to lead to rapid accretion close to channels and limited accretion far from channels. This spatial pattern has important implications for marsh vulnerability to SLR, where strong gradients in sediment supply would leave large interior sections of marshland vulnerable to drowning (Farron et al., 2020; Langston et al., 2020). The extensive ponding observed farther from channels (Figure 1c; Wilson et al., 2014) in this system is consistent with this steep gradient of sediment flux convergence. With rapid accretion close to the channel, we would expect to see a pronounced levee; however, this is absent at the site (Figure 2). This absence is likely explained by soil creep and bank slumping, which has been extensively documented in the Plum Island Estuary (Deegan et al., 2012; Mariotti et al., 2016, 2019). The slumping of the bank creates accommodation space, which would allow for increased sediment deposition without the formation of a levee (Mariotti et al., 2016, 2019). Other possible explanations for the lack of a levee could be historical changes in sediment supply associated with land clearance and dam construction (Kirwan et al., 2011) or delivery of sediment by ice rafting (Argow et al., 2011; FitzGerald et al., 2020) or major storm events that were not captured during our measurement period.

The flux convergence may also be complicated by the location of our measurements. For example, we measured SSC over the marsh, but the proportionality of flood-ebb differentials and sediment flux has only been explored in tidal channels (French et al., 2008; Ganju et al., 2017; Nowacki & Ganju, 2019). Our analysis therefore assumes that the proportionality applies to both channel and overmarsh measurements. Although initial marsh flooding occurs parallel to our transect, the proximity to a bifurcation in the channel may mean that there is lateral flow influencing the sensors at higher water levels (Figure 1c). However, our results still suggest flux convergence. The SSC in the bifurcation is likely similar to that of the main channel

and the sensors, which we consider interior to the main channel are still interior to the secondary channel (e.g., the sensor 24 m from the main channel is >20 m from the secondary channel). We would expect similar flux convergence with distance along all flow paths. In other words, lateral flow would experience the same conditions as flow parallel to the transect so we expect similar decreases in flood-ebb differential with distance, indicating flux convergence. Nonzero background concentrations observed in the marsh interior have been seen in other studies (see Christiansen et al., 2000; Poirier et al., 2017) and can be caused by numerous factors, such as lateral flow or local resuspension. Resuspension may explain the increase in channel SSC during ebb flow, but resuspension likely has a limited impact in the marsh as there is only a minor increase in marsh SSC at higher ebb velocities and only on the marsh edge. This is consistent with the limited role resuspension plays in vegetated environments (Friedrichs & Perry, 2001).

4.2. Decoupling Between Channel and Marsh Sediment Supply

Long-term, continuous measurements also allowed us to discover that marsh sediment supply is largely decoupled from channel sediment supply. Our measurements indicate that the tidal channel is the source of sediment, as evidenced by higher SSC in the channel than on the marsh and correlated fluctuations between marsh and platform SSC within tidal cycles (Figure 7). However, this coupling breaks down at time scales greater than a tidal cycle. This decoupling is present when only considering flooding tides, ebbing tides, or when considering all stages of the tidal cycle (supporting information Table S2). At larger time scales, increased concentrations in the channel do not lead to increased concentrations on the marsh (Figure 8). For example, a negative relationship between channel and marsh SSC is evident in differences from 2016 to 2017, where mean annual SSC decreased in the channel (14.9 mg/L $\pm$ 0.08 to 10.7 mg/L $\pm$ 0.09) but increased on the marsh (4.21 mg/L $\pm$ 0.05 to 6.20 mg/L $\pm$ 0.06; mean $\pm$ SE, Figure 4a). This decoupling may arise because as concentration increases in the channel, a greater proportion of sediment settles before reaching the marsh edge sensor (Figure 9b).

Decoupling between channel and marsh sediment supply was an unexpected result, and the study was not designed to determine the cause of this phenomenon. Nevertheless, we suggest two possible mechanisms to explain the greater proportional reduction in concentration when channel sediment concentrations are high (Figure 9b). The first mechanism relates to changes in sediment distribution within the channel water column, whereby the center of mass of SSC shifts downward. This could be caused by sediment in the channel beginning to settle and therefore moving downward in the water column. The lower portion of the water column, that is, where our sensor was installed, could experience an increase in concentration while the surface water SSC decreases. The mass of total suspended sediment does not necessarily change, but it is distributed differently. The marsh platform is directly interacting with surface waters and so would receive reduced sediment supply. In this case the decoupling applies specifically to near-bed channel measurements and could be mitigated by measuring water surface concentrations. A second mechanism is that settling velocity increases with increasing channel concentration. Increased settling velocity with increased concentration is likely driven by flocculation and has been well documented over a similar range of concentrations (Manning et al., 2010; Ross, 1988; Wolanski et al., 1992). In this scenario, the larger volume of sediment settles out more quickly within the channel, marsh bank, or first meter of the marsh. One recent study in the Bay of Fundy, Canada, found that increasing SSC led to increased flocculation and preferential deposition in the channel and marsh bank so that sediment deposition on the marsh did not increase with increasing channel SSC (Poirier et al., 2017). These two mechanisms would likely be connected as particle settling can cause increasing concentrations at depth and decreasing concentrations at the surface (Winterwerp, 2002).

The uniqueness of this data set means that it is challenging to determine how flux convergence and source decoupling apply to other systems. Recent work in the Bay of Fundy illustrates decoupling between the channel and marsh platform in a very high sediment, hypertidal environment (Poirier et al., 2017), but direct observations of decoupling and flux convergence elsewhere are generally limited by a lack of high-resolution SSC data on the marsh platform. We were unable to monitor the site in the winter, so it is unclear if this time period differs significantly from our conclusions. Nevertheless, the ultimate implication of flux convergence and source decoupling is that it is difficult to predict marsh vulnerability based on source-water sediment supply alone. This difficulty has been observed in a variety of environments, including microtidal salt marshes (Ganju et al., 2015), microtidal freshwater marshes (Palinkas & Engelhardt, 2018), mesotidal back-barrier marshes (Murphy & Voulgaris, 2006), hypertidal marshes (Poirier et al., 2017), and other

types of marshes (D'Alpaos & Marani, 2016; Duvall et al., 2019). Although more work is needed to determine the role of source decoupling and flux convergence in other environments, our work offers a mechanistic explanation for this phenomenon, and contributes to the growing body of literature that suggests marsh vulnerability is difficult to predict based on measurements of channel SSC alone.

5. Conclusion

Through high-resolution, long-term monitoring of SSC from a tidal channel and adjacent salt marsh, we show that channel and marsh interior SSC are largely decoupled at time scales longer than individual tidal cycles. This ultimately leads to large sections of the marsh platform that are relatively insensitive to fluctuations in channel sediment supply. Specifically, the interior of the marsh, where marsh loss often begins (Schepers et al., 2016; Zhang et al., 2019), has a minimal sediment flux and is largely decoupled from changes in channel SSC. Therefore, the vulnerability of interior marshes is not due to infrequent flooding alone and might not be easily mitigated through increased sediment concentration in the channel. Numerical and conceptual models of marsh vulnerability typically rely on channel-centric measures of sediment availability (Fagherazzi et al., 2012; Kirwan et al., 2010; Raposa et al., 2016; Ratliff et al., 2015). While it is unclear how the results apply to other systems, our work suggests that direct SSC measurements on the marsh platform may be required to adequately characterize mineral sediment availability and predict marsh vulnerability to SLR.

Data Availability Statement

Raw data for this study can be found in the Plum Island LTER data catalog (at https://pie-lter.ecosystems.mbl.edu/content/pie-lter-suspended-sediments-laws-point-west-creek-tidal-marsh-and-creek-rowley-river-rowley).

Acknowledgments

This work was funded by NSF Awards 1529245, 1654374, 1426981, 1637630, and 1832221, the NSF Graduate Research Fellowship Program, and the USGS Climate and Land Use Research and Development program. We thank D. Walters, J. Himmelstein, D. Nicks, R. Walker, T. Messerschmidt, and the Plum Island Ecosystems LTER, especially S. Kelsey for laboratory and field assistance. Additionally, we thank C. Friedrichs, G. Guntenspergen, and O. Duran Vinent for contributing ideas that helped develop the work, and the reviewers who helped improve the manuscript. This work is Contribution Number 3928 of the Virginia Institute of Marine Science. In memoriam of David Nicks.

References

Argow, B. A., Hughes, Z. J., & FitzGerald, D. M. (2011). Ice raft formation, sediment load, and theoretical potential for ice-rafted sediment influx on northern coastal wetlands. *Continental Shelf Research*, *31*(12), 1294–1305. https://doi.org/10.1016/j.csr.2011.05.004

Blum, M. D., & Roberts, H. H. (2009). Drowning of the Mississippi Delta due to insufficient sediment supply and global sea-level rise. *Nature Geoscience*, *2*(7), 488–491. https://doi.org/10.1038/ngeo553

Cavatorta, J. R., Johnston, M., Hopkinson, C., & Valentine, V. (2003). Patterns of sedimentation in a salt marsh-dominated estuary. *The Biological Bulletin*, *205*(2), 239–241. https://doi.org/10.2307/1543274

Chen, M. S., Wartel, S., & Temmerman, S. (2005). Seasonal variation of floc characteristics on tidal flats, the Scheldt estuary. *Hydrobiologia*, *540*(1–3), 181–195. https://doi.org/10.1007/s10750-004-7143-6

Christiansen, T., Wiberg, P. L., & Milligan, T. G. (2000). Flow and sediment transport on a tidal salt marsh surface. *Estuarine, Coastal and Shelf Science*, *50*(3), 315–331. https://doi.org/10.1006/ecss.2000.0548

Coleman, D. J., & Kirwan, M. L. (2019). The effect of a small vegetation dieback event on salt marsh sediment transport. *Earth Surface Processes and Landforms*, *44*(4), 944–952. https://doi.org/10.1002/esp.4547

D'Alpaos, A., & Marani, M. (2016). Reading the signatures of biologic-geomorphic feedbacks in salt-marsh landscapes. *Advances in Water Resources*, *93b*, 265–275. https://doi.org/10.1016/j.advwatres.2015.09.004

Day, J. W., Boesch, D. F., Clairain, E. J., Kemp, G. P., Laska, S. B., Mitsch, W. J., et al. (2007). Restoration of the Mississippi Delta: Lessons from Hurricane Katrina and Rita. *Science*, *315*(5819), 1679–1684. https://doi.org/10.1126/science.1137030

Deegan, L. A., Johnson, D. S., Warren, R. S., Peterson, B. J., Fleeger, J. W., Fagherazzi, S., & Wollheim, W. M. (2012). Coastal eutrophication as a driver of salt marsh loss. *Nature*, *490*(7420), 388–392. https://doi.org/10.1038/nature11533

Dickhudt, P. J., Friedrichs, C. T., Schaffner, L. C., & Sanford, L. P. (2009). Spatial and temporal variation in cohesive sediment erodibility in the York River estuary, eastern USA: A biologically influenced equilibrium modified by seasonal deposition. *Marine Geology*, *267*(3–4), 128–140. https://doi.org/10.1016/j.margeo.2009.09.009

Duvall, M. S., Wiberg, P. L., & Kirwan, M. L. (2019). Controls on sediment suspension, flux, and marsh deposition near a bay-marsh boundary. *Estuaries and Coasts*, *42*(2), 403–424. https://doi.org/10.1007/s12237-018-0478-4

Ellison, J. C., & Stoddart, D. R. (1991). Mangrove ecosystem collapse during predicted sea-level rise: Holocene analogues and implications. *Journal of Coastal Research*, *7*(1), 151–165. https://www.jstor.org/stable/4297812

Fagherazzi, S., Kirwan, M. L., Mudd, S. M., Guntenspergen, G. R., Temmerman, S., D'Alpaos, A., et al. (2012). Numerical models of salt marsh evolution: Ecological, geomorphic, and climatic factors. *Reviews of Geophysics*, *50*, RG1002. https://doi.org/10.1029/2011RG000359

Farron, S. J., Hughes, Z. J., & FitzGerald, D. M. (2020). Assessing the response of the Great Marsh to sea-level rise: Migration, submersion or survival. *Marine Geology*, *425*, 106195. https://doi.org/10.1016/j.margeo.2020.106195

Fitzgerald, D. M., Buynevich, I., & Argow, B. (2006). Model of tidal inlet and barrier island dynamics in a regime of accelerated sea level rise. *Journal of Coastal Research*, *39*(II), 789–795. https://www.jstor.org/stable/25741684

FitzGerald, D. M., Hughes, Z. J., Georgiou, I. Y., Black, S., & Novak, A. (2020). Enhanced, climate-driven sedimentation on salt marshes. *Geophysical Research Letters*, *47*, e2019GL086737. https://doi.org/10.1029/2019GL086737

French, J. R., Burningham, H., & Benson, T. (2008). Tidal and meteorlogical forcings of suspended sediment flux in a muddy, mesotidal estuary. *Estuaries and Coasts*, *31*(5), 843–859. https://doi.org/10.1007/s12237-008-9072-5

Friedrichs, C. T., & Perry, J. E. (2001). Tidal salt marsh morphodynamics: A synthesis. *Journal of Coastal Research*, *27*, 7–37. https://www.jstor.org/stable/25736162

Ganju, N. K., Defne, Z., Kirwan, M. L., Fagherazzi, S., D'Alpaos, A., & Carniello, L. (2017). Spatially integrative metrics reveal hidden vulnerability of microtidal salt marshes. *Nature Communications*, *8*(1), 14156. https://doi.org/10.1038/ncomms14156

Ganju, N. K., Kirwan, M. L., Dickhudt, P. J., Guntenspergen, G. R., Cahoon, D. R., & Kroeger, K. D. (2015). Sediment transport-based metrics of wetland stability. *Geophysical Research Letters*, *42*, 7992–8000. https://doi.org/10.1002/2015GL065980

Ganju, N. K., Schoellhamer, D. H., & Bergamaschi, B. A. (2005). Suspended sediment fluxes in a tidal wetland: Measurement, controlling factors, and error analysis. *Estuaries*, *28*(6), 812–822. https://doi.org/10.1007/BF02696011

Giblin, A. (2017). Year 2016, meteorological data, 15 minute intervals, from the PIE LTER Marshview Farm weather station located in Newbury, MA Environmental Data Initiative. https://doi.org/10.6073/pasta/d5bfbfc6de185cff9b7302884c78e0fe

Giblin, A. (2018). Year 2017, meteorological data, 15 minute intervals, from the PIE LTER Marshview Farm weather station located in Newbury, MA Environmental Data Initiative. https://doi.org/10.6073/pasta/80e0962b53d2549002fcc53eaf7394c6

Gunnell, J. R., Rodriguez, A. B., & McKee, B. A. (2013). How a marsh is built from the bottom up. *Geology*, *41*(8), 859–862. https://doi.org/10.1130/G34582.1

Harris, C. K., Sherwood, C. R., Signell, R. P., Bever, A. J., & Warner, J. C. (2008). Sediment dispersal in the northwestern Adriatic Sea. *Journal of Geophysical Research*, *113*, C11S03. https://doi.org/10.1029/2006JC003868

Hopkinson, C. S., Morris, J. T., Fagherazzi, S., Wollheim, W. M., & Raymond, P. A. (2018). Lateral marsh edge erosion as a source of sediments for vertical marsh accretion. *Journal of Geophysical Research: Biogeosciences*, *123*, 2444–2465. https://doi.org/10.1029/2017JG004358

Jankowski, K. L., Tornqvist, T. E., & Fernandes, A. M. (2017). Vulnerability of Louisiana's coastal wetlands to present-day rates of relative sea-level rise. *Nature Communications*, *8*(1), 14792. https://doi.org/10.1038/ncomms14792

Kirwan, M. L., Guntenspergen, G. R., D'Alpaos, A., Morris, J. T., Mudd, S. M., & Temmerman, S. (2010). Limits on the adaptability of coastal marshes to rising sea level. *Geophysical Research Letters*, *37*, L23401. https://doi.org/10.1029/2010GL045489

Kirwan, M. L., Murray, A. B., Donnelly, J. P., & Corbett, D. R. (2011). Rapid wetland expansion during European settlement and its implication for marsh survival under modern sediment delivery rates. *Geology*, *39*(5), 507–510. https://doi.org/10.1130/G31789.1

Langston, A. K., Durán Vinent, O., Herbert, E. R., & Kirwan, M. L. (2020). Modeling long-term salt marsh response to sea level rise in the sediment-deficient Plum Island Estuary, MA. *Limnology and Oceanography*. https://doi.org/10.1002/lno.11444

Leonard, L. A., & Reed, D. J. (2002). Hydrodynamics and sediment transport through tidal marsh canopies. *Journal of Coastal Research*, *36*, 459–469. https://doi.org/10.2112/1551-5036-36.sp1.459

Li, H., & Yang, S. L. (2009). Trapping effect of tidal marsh vegetation on suspended sediment, Yangtze Delta. *Journal of Coastal Research*, *254*(4), 915–924. https://doi.org/10.2112/08-1010.1

Manning, A. J., Langston, W. J., & Jonas, P. J. C. (2010). A review of sediment dynamics in the Severn Estuary: Influence of flocculation. *Marine Pollution Bulletin*, *61*(1–3), 37–51. https://doi.org/10.1016/j.marpolbul.2009.12.012

Mariotti, G., Kearney, W. S., & Fagherazzi, S. (2016). Soil creep in salt marshes. *Geology*, *44*(6), 459–462. https://doi.org/10.1130/G37708.1

Mariotti, G., Kearney, W. S., & Fagherazzi, S. (2019). Soil creep in a mesotidal salt marsh channel bank: Fast, seasonal, and water table mediated. *Geomorphology*, *334*, 126–137. https://doi.org/10.1016/j.geomorph.2019.03.001

Millette, T. L., Argow, B. A., Marcano, E., Hayward, C., Hopkinson, C. S., & Valentine, V. (2010). Salt marsh geomorphical analyses via integration of multitemporal multispectral remote sensing with LIDAR and GIS. *Journal of Coastal Research*, *265*(265), 809–816. https://doi.org/10.2112/JCOASTRES-D-09-00101.1

Morris, J. T., Barber, D. C., Callaway, J. C., Chambers, R., Hagen, S. C., Hopkinson, C. S., et al. (2016). Contributions of organic and inorganic matter to sediment volume and accretion in tidal wetlands at steady state. *Earth's Future*, *4*(4), 110–121. https://doi.org/10.1002/2015EF000334

Moskalski, S. M., & Sommerfield, C. K. (2012). Suspended sediment deposition and trapping efficiency in a Delaware salt marsh. *Geomorphology*, *139-140*, 195–204. https://doi.org/10.1016/j.geomorph.2011.10.018

Murphy, S., & Voulgaris, G. (2006). Identifying the role of tides, rainfall and seasonality in marsh sedimentation using long-term suspended sediment concentration data. *Marine Geology*, *227*(1–2), 31–50. https://doi.org/10.1016/j.margeo.2005.10.006

Nowacki, D. J., & Ganju, N. K. (2019). Simple metrics predict salt-marsh sediment fluxes. *Geophysical Research Letters*, *46*, 12,250–12,257. https://doi.org/10.1029/2019GL083819

Palinkas, C. M., & Engelhardt, K. A. M. (2018). Influence of inundation and suspended-sediment concentrations on spatiotemporal sedimentation patterns in a tidal freshwater marsh. *Wetlands*, *39*(3), 507–520. https://doi.org/10.1007/s13157-018-1097-3

Poirier, E., van Proosdij, D., & Milligan, T. G. (2017). The effect of source suspended sediment concentration on the sediment dynamics of a macrotidal creek and salt marsh. *Continental Shelf Research*, *148*, 130–138. https://doi.org/10.1016/j.csr.2017.08.017

Raposa, K. B., Wasson, K., Smith, E., Crooks, J. A., Delgado, P., Fernald, S. H., et al. (2016). Assessing tidal marsh resilience to sea-level rise at broad geographic scales with multi-metric indices. *Biological Conservation*, *204*, 263–275. https://doi.org/10.1016/j.biocon.2016.10.015

Ratliff, K. M., Braswell, A. E., & Marani, M. (2015). Spatial response of coastal marshes to increased atmospheric CO_2. *Proceedings of the National Academy of Sciences*, *112*(51), 15,580–15,584. https://doi.org/10.1073/pnas.1516286112

Reed, D. J., Spencer, T., Murray, A. L., French, J. R., & Leonard, L. (1999). Marsh surface sediment deposition and the role of tidal creeks: Implications for created and managed coastal marshes. *Journal of Coastal Conservation*, *5*(1), 81–90. https://doi.org/10.1007/BF02802742

Ross, M. A. (1988). Vertical structure of estuarine fine sediment suspensions. PhD. Dissertation University of Florida. 206p.

Schepers, L., Kirwan, M. L., Guntenspergen, G., & Temmerman, S. (2016). Spatio-temporal development of vegetation die-off in a submerging coastal marsh. *Limnology and Oceanography*, *62*(1), 137–150. https://doi.org/10.1002/lno.10381

Syvitski, J. P. M., Kettner, A. J., Overeem, I., Hutton, E. W. H., Hannon, M. T., Brakenridge, G. R., et al. (2009). Sinking deltas due to human activities. *Nature Geoscience*, *2*(10), 681–686. https://doi.org/10.1038/ngeo629

Temmerman, S., Bouma, T. J., Govers, G., Wang, Z. B., de Vries, M. B., & Herman, P. M. J. (2005). Impact of vegetation on flow routing and sedimentation patterns: Three-dimensional modeling for a tidal marsh. *Journal of Geophysical Research*, *110*, F04019. https://doi.org/10.1029/2005JF000301

Tommasini, L., Carniello, L., Ghinassi, M., Roner, M., & D'Alpaos, A. (2019). Changes in the wind-wave field and related saltmarsh lateral erosion: Inferences from the evolution of the Venice Lagoon in the last four centuries. *Earth Surface Processes and Landforms*, *44*(8), 1633–1646. https://doi.org/10.1002/esp.4599

Tweel, A. W., & Turner, R. E. (2012). Landscape-scale analysis of wetland sediment deposition from four tropical cyclone events. *PLoS ONE*, *7*(11), e50528. https://doi.org/10.1371/journal.pone.0050528

Voulgaris, G., & Meyers, S. T. (2004). Temporal variability of hydrodynamics, sediment concentration and sediment settling velocity in a tidal creek. *Continental Shelf Research*, *24*(15), 1659–1683. https://doi.org/10.1016/j.csr.2004.05.006

Wang, F. C., Lu, T., & Sikora, W. B. (1993). Intertidal marsh suspended sediment transport processes, Terrebonne Bay, Louisiana, U.S.A. *Journal of Coastal Research*, *9*(1), 209–220. https://www.jstor.org/stable/4298078

Weston, N. B. (2014). Declining sediments and rising seas: An unfortunate convergence for tidal wetlands. *Estuaries and Coasts*, *37*(1), 1–23. https://doi.org/10.1007/s12237-013-9654-8

Wilson, C. A., Hughes, Z. J., Fitzgerald, D. M., Hopkinson, C. S., Valentine, V., & Kolker, A. S. (2014). Saltmarsh pool and tidal creek morphodynamics: Dynamic equilibrium of northern latitude saltmarshes? *Geomorphology*, *213*, 99–115. https://doi.org/10.1016/j.geomorph.2014.01.002

Winterwerp, J. C. (2002). On the flocculation and settling velocity of estuarine mud. *Continental Shelf Research*, *22*(9), 1339–1360. https://doi.org/10.1016/S0278-4343(02)00010-9

Wolanski, E., Gibbs, R. J., Mazda, Y., Mehta, A., & King, B. (1992). The role of turbulence in the settling of mud flocs. *Journal of Coastal Research*, *8*(1), 35–46. https://www.jstor.org/stable/4297950

Zhang, X., Leonardi, N., Donatelli, C., & Fagherazzi, S. (2019). Fate of cohesive sediments in a marsh-dominated estuary. *Advances in Water Resources*, *125*, 32–40. https://doi.org/10.1016/j.advwatres.2019.01.003